Electrical transport, magnetic, and electronic structure studies of $Mg_{0.95}Mn_{0.05}Fe_{2-2x}Ti_{2x}O_{4 \pm \delta}$ $(0 \leq x \leq 0.5)$ ferrites

2007 J. Phys.: Condens. Matter 19 476210

(http://iopscience.iop.org/0953-8984/19/47/476210)

IOP PUBLISHING JOURNAL OF PHYSICS: CONDENSED MATTER

J. Phys.: Condens. Matter **19** (2007) 476210 (15pp) doi:10.1088/0953-8984/19/47/476210

Electrical transport, magnetic, and electronic structure studies of $Mg_{0.95}Mn_{0.05}Fe_{2-2x}Ti_{2x}O_{4\pm\delta}$ ($0 \leqslant x \leqslant 0.5$) ferrites

Shalendra Kumar[1], Alimuddin[1], Ravi Kumar[2], P Thakur[3], K H Chae[3], Basavaraj Angadi[4] and W K Choi[4]

[1] Department of Applied Physics, Aligarh Muslim University, Aligarh 202002, India
[2] Materials Science Division, Inter University Accelerator Centre, Aruna Asaf Ali Marg, New Delhi 110067, India
[3] Materials Science and Technology Research Division, KIST, Seoul 136-791, Korea
[4] Thin Film Materials Research Center, KIST, Seoul 136-791, Korea

Received 20 July 2007, in final form 21 September 2007
Published 1 November 2007
Online at stacks.iop.org/JPhysCM/19/476210

Abstract

We present structural, electrical transport, magnetic, and electronic structure studies of $Mg_{0.95}Mn_{0.05}Fe_{2-2x}Ti_{2x}O_4$ ferrite using x-ray diffraction, dielectric spectroscopy, DC magnetization and near edge x-ray absorption fine structure (NEXAFS) measurements. The x-ray diffraction study shows a structural transition from cubic to tetragonal with Ti substitution. The dielectric constant and DC conductivity increase with Ti substitution up to $x = 0.2$. However, with further increase of substitution both the dielectric constant and DC conductivity decrease. This electrical behavior indicates that at low values of substitution, hopping between Fe^{3+} and Fe^{2+} increases whereas at higher concentrations the total content of Fe ions decreases. It is observed that all the samples exhibit ferrimagnetic behavior at 300 K and the saturation magnetization decreases with increase in Ti substitution. The NEXAFS measurements have been carried out at O K-, Fe L-, Fe K-, and Ti L-edges to investigate the chemical states and the electronic structure of the $Mg_{0.95}Mn_{0.05}Fe_{2-2x}Ti_{2x}O_4$ ($0 \leqslant x \leqslant 0.5$) system at room temperature. The O K-edge spectra indicate that the Fe 3d orbitals are considerably modified with the substitution of Ti ions. At $x \geqslant 0.3$, a new spectral feature appears (~532 eV) due to the transitions from oxygen 2p to Ti 3d orbitals which starts dominating the pre-edge spectra of the system. Both Fe $L_{3,2}$- and Fe K-edge spectra indicate that iron Fe^{3+} ions convert into Fe^{2+} with the substitution of Ti ions. The Ti $L_{3,2}$-edge NEXAFS spectra reveal that the Ti remains in the 4+ state for all the samples. The observed experimental results have been explained on the basis of dilution of the magnetic sublattice by Ti substitution, which provides a strong interplay between electrical and magnetic properties along with their electronic structure.

1. Introduction

Ferrites are well studied materials, but due to the large interest in various potential applications and in order to understand the ongoing physical processes to tailor make these materials for modern technology, there has been a growing interest in the study of magnetic, electric, and structural properties of mixed spinel ferrites [1–6]. The basis for the wide range of applications is related to the variety of transition metal cations which can be incorporated into the lattice of the parent magnetic structure. Spinel ferrites crystallize into a cubic close packed structure of oxygen ions. The cations occupy two types of interstitial sites. One of them is called a tetrahedral (A) site with the cation surrounded by the four oxygen ions in tetrahedral coordination. The other interstitial position is known as an octahedral (B) site with a cation coordinated by six oxygen ions in octahedral symmetry. In general, the cation distribution in the spinel lattice has the form: $(A_{1-x}M_x)$ $[A_xM_{2-x}]$ O_4, where A and M are divalent and trivalent ions, respectively and x is the so-called degree of inversion. The round and square brackets denote the cations located at the center of the tetrahedral lattice of oxygen (A) and those at the octahedral (B) lattice, respectively. The origin of the magnetic properties of spinel oxides is the spin magnetic moment of the unpaired 3d electrons of the transition element coupled by the superexchange interaction via the oxygen ions separating them. The magnetic properties of spinel ferrites, such as transition temperature and saturation magnetic moment are strongly dependent on the distribution of cations and type of doping atom. These materials seem to be smart and show a variety of magnetic structures [7–12].

Many research groups have studied the effect of tetravalent substitution in different ferrite matrices to upgrade their structural, electrical, and magnetic properties. The effect of the substitution of Ti ions on the magnetic, electric, and dielectric properties of ferrites has been extensively studied by many authors [13–17]. Brand *et al* [14] found in the case of $Mg_{1+x}Ti_xFe_{2-2x}O_4$ that on increasing dilution x, the collinear ferrimagnetic phase breaks down before reaching the ferrimagnetic percolation threshold and for the higher concentration of Ti, the system approaches a spin-glass. Dormann *et al* [6] have also studied the magnetization measurements of Ti^{4+} substituted lithium ferrite using different techniques and suggested the possibility of a canted spin arrangement to explain the magnetization measurements. It was observed that substitution of Ti ions in Mg–Zn ferrite [15] and Li ferrite [16] reduces their electrical conductivity. Also in Ni–Zn ferrite, the Ti substitution reduced their dielectric constant and dielectric loss [17]. In the present work we have studied the effect of the doping of Ti^{4+} ions in Mg–Mn ferrite and found that up to 50% system exhibits a ferrimagnetic ordering at room temperature and dielectric constant, DC and AC conductivity increased with the substitution of Ti ions up to 20% and then decreased systematically with further substitution. In NEXAFS studies, the O K-edge spectra clearly indicate that the Fe 3d orbitals are considerably modified with the dilution of Ti. The Fe L- and K-edges spectra demonstrate the coexistence of Fe^{2+}–Fe^{3+} ions and conversion of Fe^{3+} to Fe^{2+} ions with the substitution of Ti ions.

In the present paper, we present the effect of Ti substitution at the Fe site (B-site) in Mg–Mn ferrites on their electrical transport and magnetic properties. To validate our observations, we have also investigated the electronic structure of Ti substituted Mg–Mn ferrite by near edge x-ray absorption fine structure measured at O K-, Fe K-, Fe $L_{3,2}$-, and Ti $L_{3,2}$-edges. The Ti 2p NEXAFS spectra reveal that the valency of Ti remains at 4+.

2. Experimental details

Single phase polycrystalline bulk samples of $Mg_{0.95}Mn_{0.05}Fe_{2-2x}Ti_{2x}O_4$ were synthesized using a standard solid-state reaction technique. The stoichiometric amounts of highly pure

MgO, FeO, MnO_2 and TiO_2 powders were mixed thoroughly and pre-calcinated for 12 h at 1000 °C. The pre-calcinated materials were again ground and calcinated at 1250 °C for 24 h. Finally, the samples were ground to fine powder, pressed into circular pellets by applying a pressure of 5 tonnes and then sintered at 1300 °C for 24 h. Powder x-ray diffraction (XRD) was performed at room temperature using a Bruker AXE D8 x-ray powder diffractometer with Cu Kα radiation. The dielectric measurements were carried out using an Agilent 4284A precision LCR meter at room temperature in the frequency range from 75 kHz to 5 MHz. Shielded test leads were used for the electrical connections from the LCR meter to the sample in order to avoid any parasitic impedance. Before starting the measurements the samples were heated at 100 °C for 1 h, so as to homogenize the charge carriers and to remove the moisture content therein. The surfaces of the disks were polished and coated with silver paste; they acted as good contacts and electrodes for measuring the dielectric properties.

The value of the dielectric constant (ε') of these samples is calculated using the formula

$$\varepsilon' = \frac{C \times t}{\varepsilon_0 \cdot A}, \tag{1}$$

where ε_0 is the permittivity in vacuum equal to 8.854×10^{-12} C^2 N^{-1} m^{-2}, C is the capacitance of the specimen, t is the sample thickness and A is the area of the specimen in square meters. The ac conductivity is calculated from the data of the dielectric constant and loss tangent ($\tan\delta$) using the relation

$$\sigma_{AC} = \varepsilon' \varepsilon_0 \omega \tan\delta, \tag{2}$$

where $\omega = 2\pi f$ and $\tan\delta$ is the loss tangent, proportional to the 'loss' of energy from the applied field into the sample (in fact this energy is dissipated into heat) and therefore denoted as dielectric loss.

The DC conductivity of the samples was measured using a Keithley electrometer (Model 617) in the temperature range 250–400 K. The temperature was controlled with an accuracy of 50 mK using Lakeshore (Model 340) temperature controller. Magnetic measurements were made using a home made vibrating sample magnetometer [18] and the temperature was controlled to an accuracy of 0.01 K using commercial Lakeshore controllers DCR93CA. The NEXAFS measurements of these samples along with the reference compounds of Fe_2O_3, FeO and TiO_2 at O K-, Fe $L_{3,2}$-, and Ti $L_{3,2}$-edges were performed at the soft x-ray beam line 7B1 KIST of the Pohang Accelerator Laboratory (PAL), operating at 2.5 GeV with a maximum storage current of 200 mA. All the samples were scraped with diamond foil prior to the measurements in order to remove any surface contaminants. The spectra were simultaneously collected in the total electron yield (TEY) mode and the fluorescence yield (FY) mode at room temperature in a vacuum better than 1.5×10^{-8} Torr. The spectra in the two modes turned out to be nearly identical, indicating that the systems are so stable that the surface contamination effects are negligible even in the TEY mode. The spectra were normalized to incident photon flux and the energy resolution was better than 0.2 eV. For Fe K-edge experiments, BL7C1 beamline of the PAL was utilized. The beam was monochromatized by a double-crystal Si(111) monochromator detuned from 20 to 30%, to suppress higher-order harmonic content from the beam. All the scans were made in transmission mode with nitrogen–argon gas-filled ionization chambers as detectors. The Fe K-edge energy, 7112 eV, was calibrated using the first inflection point of the edge region of a metallic Fe foil. The resolution of the monochromator was about 1.5 eV in the energy range studied.

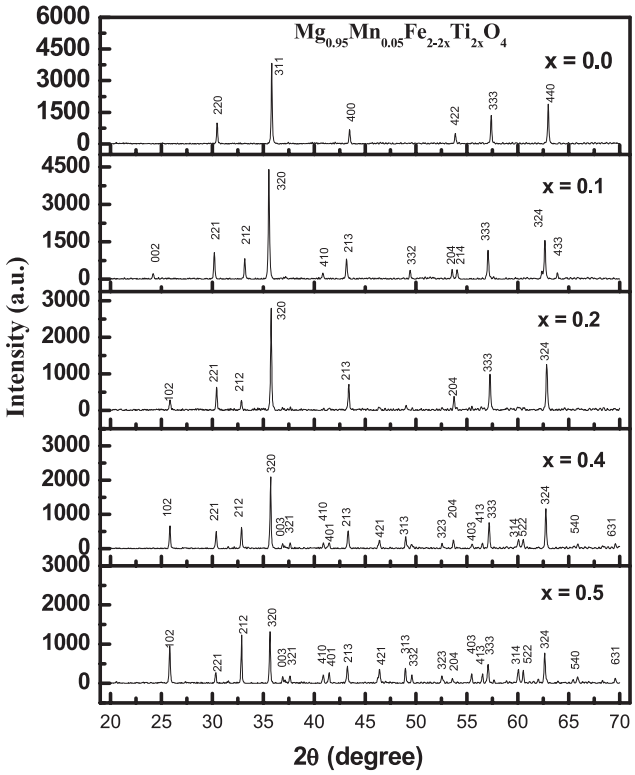

Figure 1. Powder x-ray diffraction patterns of $Mg_{0.95}Mn_{0.05}Fe_{2-2x}Ti_{2x}O_4$ samples at 300 K.

Table 1. Lattice parameter, unit cell volume, and frequency exponent (s) activation energy and magneton number of $Mg_{0.95}Mn_{0.05}Fe_{2-2x}Ti_{2x}O_4$ ($0 \leqslant x \leqslant 0.5$) samples.

	Parameters/Conc. (x)				
	0.0	0.1	0.2	0.4	0.5
$a = b$ (Å)	$a = 8.335$	9.0339	9.044	9.0478	9.053
c (Å)	$a = 8.335$	7.3458	7.325	7.321	7.320
a/c	1.0	1.229	1.234	1.235	1.237
Volume (Å^3)	579.912	597.803	598.813	599.235	599.923
Frequency exponent, s	0.582	0.743	0.740	0.787	0.690
Activation energy, E (eV)	0.318	0.242	0.174	0.204	0.227
Magneton number, n_B (μ_B)	0.44	0.32	0.26	0.19	0.12

3. Results and discussion

3.1. X-ray diffraction

Figure 1 shows the powder x-ray diffraction pattern of $Mg_{0.95}Mn_{0.05}Fe_{2-2x}Ti_{2x}O_4$ ($0 \leqslant x \leqslant 0.5$) ferrite samples. All the samples exhibit a single phase nature with structural transformation from cubic spinel to tetragonal on substitution of Ti. The variation in lattice parameters extracted using Powder-X software is shown in table 1. This structural transformation is attributed to the replacement of Ti^{4+} (0.64 Å) with the Fe^{3+} (0.67 Å) ions at B-site,

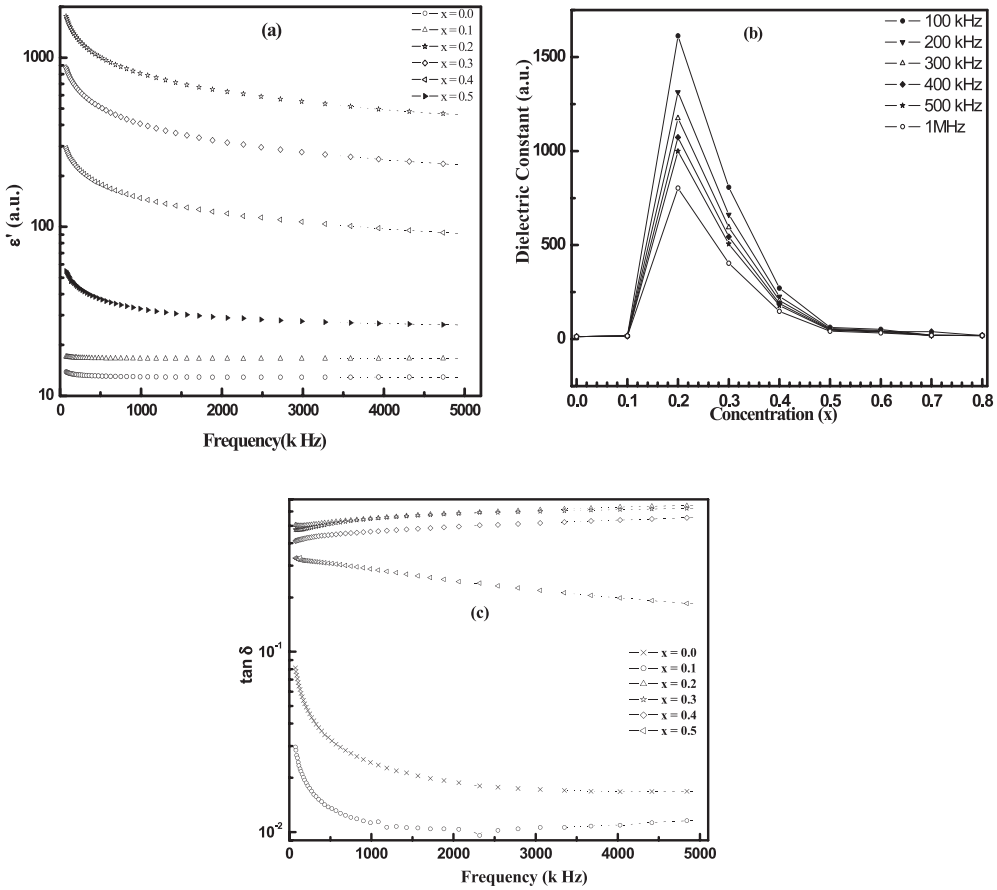

Figure 2. (a) Dielectric constant as a function of frequency of the $Mg_{0.95}Mn_{0.05}Fe_{2-2x}Ti_{2x}O_4$ samples at room temperature. (b) Dielectric constant as a function of composition of the $Mg_{0.95}Mn_{0.05}Fe_{2-2x}Ti_{2x}O_4$ samples at room temperature. (c) Loss tangent ($\tan\delta$) as a function of frequency of the $Mg_{0.95}Mn_{0.05}Fe_{2-2x}Ti_{2x}O_4$ samples at room temperature.

consequently, Ti^{4+} ions move from the center of octahedra and distort the octahedral symmetry. It is also clear from the calculated lattice parameter values that the Ti ions stretch the unit cell along the a, b axis and contract along the c axis. It is evident from the XRD analysis that unit cell volume increases from 579.91 to 599.92 $Å^3$ (shown in table 1) with doping of Ti ions due to the formation of Fe^{2+} (0.83 Å) ions to maintain the charge neutrality in the system.

3.2. Electrical properties

3.2.1. Dielectric constant behavior. Figure 2(a) shows the dielectric constant as a function of frequency for $Mg_{0.95}Mn_{0.05}Fe_{2-2x}Ti_{2x}O_4$ ($0 \leqslant x \leqslant 0.5$) at room temperature in the frequency range 75 kHz–5 MHz. It is observed that all studied samples exhibit dispersion behavior i.e. the dielectric constant decreases with increase in the frequency. This is the general dielectric behavior observed in most of the ferrite materials, which can be explained by the interfacial polarization predicted by the Maxwell–Wagner model [20] in agreement with Koop's phenomenological theory [21]. According to these models, the dielectric materials can

be imagined as a heterogeneous structure consisting of well conducting grains separated by a thin layer of poorly conducting substances (grain boundaries). These grain boundaries could be formed during the sintering process either by superficial reduction or oxidation of crystallites in the porous materials as a result of their direct contact with the firing atmosphere [22]. The grain boundaries of the lower conductivity were found to be effective at lower frequencies while grains of high conductivity are effective at high frequencies [17, 21, 23, 24]. In this case, the applied voltage on the sample drops mainly across the grain boundaries, which results in building up the space charge polarization depending upon the available free charge carriers. The observed decrease in the value of dielectric constant with increasing frequency may be attributed to the fact that the electron exchange between Fe^{2+} and Fe^{3+} ions cannot follow the change of the external applied field beyond a certain frequency.

The compositional variation of the dielectric constant at 100 kHz is shown in figure 2(b). It is observed that the dielectric constant increases with an increase in the Ti concentration up to 20% then decreases afterwards. In Mg–Mn ferrites, Fe ions occupy the tetrahedral (A) as well as the octahedral (B) sites respectively. When Ti^{4+} ions are substituted in place of Fe^{3+} ions, some of the iron is converted into Fe^{2+} in order to maintain the charge neutrality in the system, which is also clear from the x-ray diffraction, where the unit cell volume increases with the substitution (see table 1). Initially, doping of Ti increases the hopping in between Fe^{3+} and Fe^{2+} ions, thereby decreasing t he resistance of the grain. The probability of reaching the electron at the grain boundary is, thus, enhanced. As a result, the polarization and hence, the dielectric constant increase. The dielectric constant has a maximum value at a doping level of 20% because with further substitution of Ti ions, the total concentration of Fe ions itself is decreasing, hence the dielectric constant starts decreasing. Figure 2(c) shows the variation of the loss tangent as a function of frequency of all the samples. It is clear from figure 2(c) that the dielectric loss tangent ($\tan\delta$) is very low for pure and $x = 0.1$ and decreases with increase in frequency, whereas for higher substitution values, it is almost independent of frequency.

3.2.2. AC conductivity. The AC conductivity calculated using equation (2) for samples over a wide frequency range (75 kHz–5 MHz) at room temperature is shown in figure 3(a). It is observed that AC conductivity increases sharply at low frequencies and slowly at higher frequencies. The electrical conduction mechanism in the samples can be explained using the electron hopping model suggested by Heikes and Johnson [19]. According to this model, the conduction could be due to the electrons hopping between two nearest octahedral sites (B-sites) in the spinel lattice and a hopping of electrons between $Fe^{2+} \leftrightarrow Fe^{3+}$ ions. It is clear from figure 3(a) that the AC conductivity increases with the doping and exhibits a maximum for 20% doping. This indicates that the hopping of the charge between $Fe^{2+} \leftrightarrow Fe^{3+}$ ions at the octahedral site is maximum for 20% doping and decreases due to the reduction in the concentration of Fe ions in the system at the higher doping percentages. In general, for granular oxide ceramic materials, the AC conductivity follows a power law behavior with frequency given by [25, 26]:

$$\sigma_{AC} = A\omega^s, \tag{3}$$

where A is a constant having the unit of the conductivity, the exponent 's' is a dimensionless parameter and ω is the angular frequency at which the conductivity was measured. In the present case, 's' was calculated for all compositions at room temperature over the studied range of frequency by plotting $\ln\sigma_{AC}$ versus $\ln\omega$, according to equation (3) shown in figure 3(b). The exponent s is a measure of the degree of correlation, i.e. s should be zero for random hopping and tends to one as the correlation increases. Table 1 shows the value of 's' for all the samples. In the present systems the observed 's' values lie between 0.5 and 0.8, indicating a strong

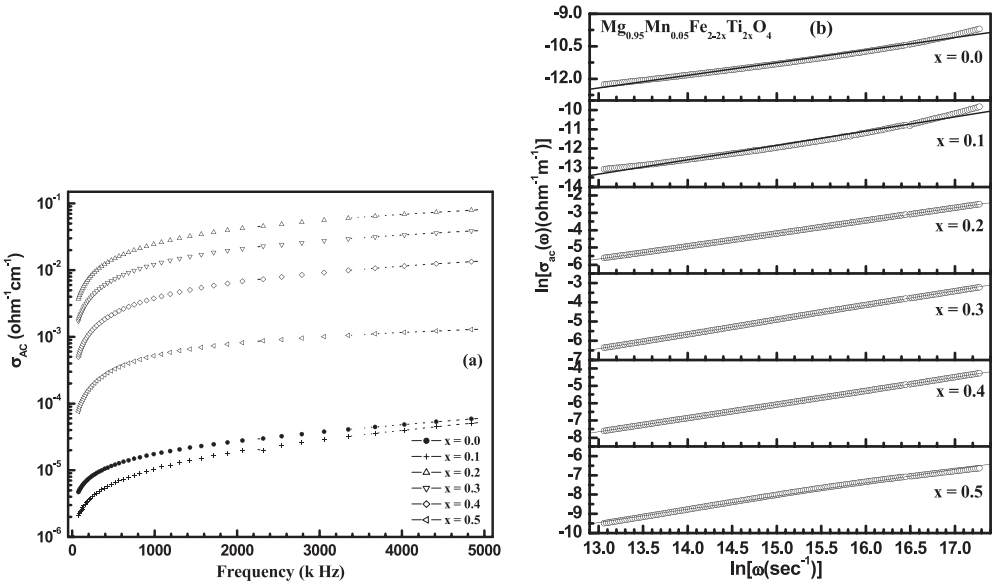

Figure 3. (a) AC conductivity as a function of frequency of the $Mg_{0.95}Mn_{0.05}Fe_{2-2x}Ti_{2x}O_4$ samples. (b) Variation of log σ and log ω of the $Mg_{0.95}Mn_{0.05}Fe_{2-2x}Ti_{2x}O_4$ samples at room temperature.

correlation of electrons in these systems. Our results are in good agreement with the reported results of other workers [27, 28].

3.2.3. Temperature dependence of the DC conductivity. The effect of temperature on the DC electrical conductivity of $Mg_{0.95}Mn_{0.05}Fe_{2-2x}Ti_{2x}O_4$ ($0 \leqslant x \leqslant 0.5$) ferrites has been investigated from 250 to 400 K and is shown in figure 4(a). The electrical conductivity σ increases with temperature, T. This can be attributed to the increase in the drift mobility of electric charge carriers, which are thermally activated upon increasing the temperature. The observed increase in σ with temperature is similar to the semiconductor behavior, which follows the Arrhenius relation,

$$\sigma T = \sigma_0 \exp \frac{-E_a}{kT}, \tag{4}$$

where σ_0 is the pre-exponential factor with dimensions of Ω^{-1} cm^{-1} K, E_a is the activation energy for the electrical conduction and k is the Boltzmann constant. The activation energy has been calculated from the plot of log ($\sigma_{DC}T$) versus temperature ($10^3/T$) and is shown in table 1. From table 1, it is clear that activation energy decreases with substitution of Ti ions and has a minimum value at 20% doping due to the decrease in the resistance of grains. Figure 4(b) shows the DC conductivity as a function of composition and indicates that the DC conductivity increases with doping of Ti ions up to 20% and then starts decreasing with further doping. These results are also consistent with the AC conductivity and dielectric constant.

3.3. Magnetic properties

Figure 5 shows the isothermal DC magnetization hysteresis loops of $Mg_{0.95}Mn_{0.05}Fe_{2-2x}Ti_{2x}O_4$ ($0 \leqslant x \leqslant 0.5$) at 300 K. It is clearly evident from figure 5 that all the samples show ferrimagnetic behavior above room temperature and the value of saturation magnetization decreases

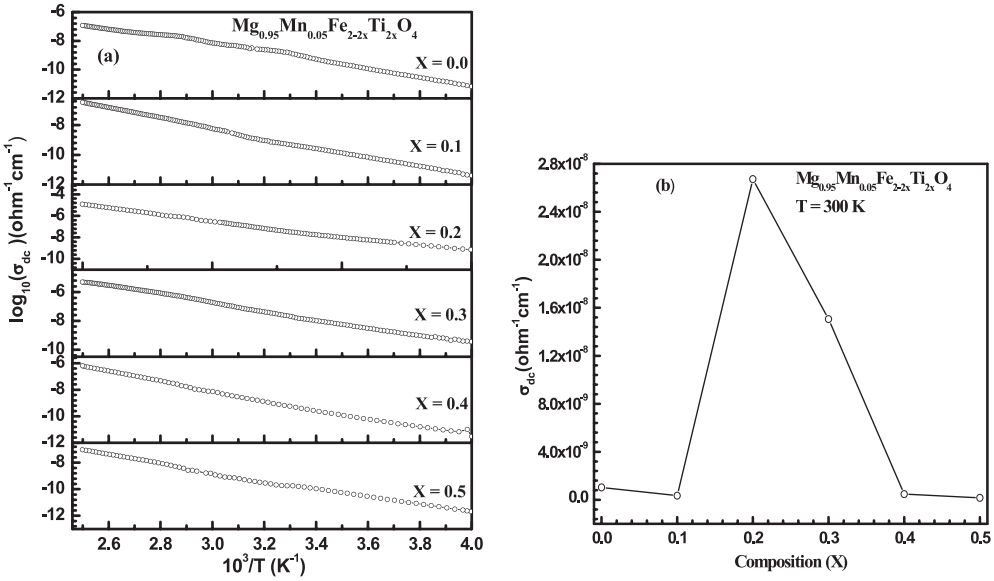

Figure 4. (a) DC conductivity as a function of the temperature of the $Mg_{0.95}Mn_{0.05}Fe_{2-2x}Ti_{2x}O_4$ samples. (b) DC conductivity as a function of the composition of the $Mg_{0.95}Mn_{0.05}Fe_{2-2x}Ti_{2x}O_4$ samples at 300 K.

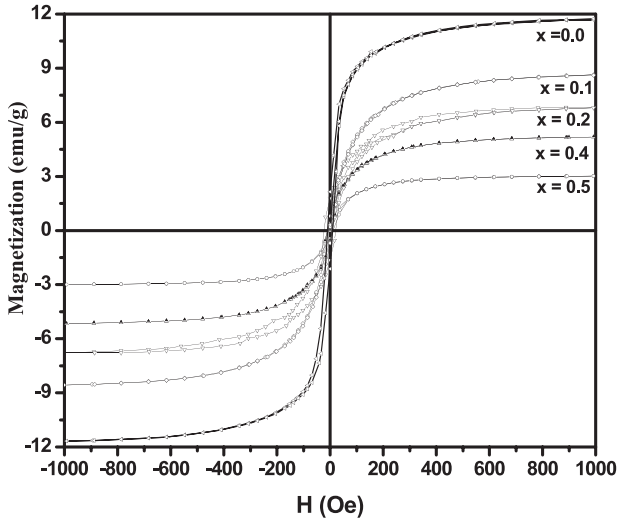

Figure 5. Magnetization hysteresis of $Mg_{0.95}Mn_{0.05}Fe_{2-2x}Ti_{2x}O_4$ as a function of magnetic field at 300 K.

with the increase in the concentration of Ti ions. Further, we have also calculated, the magneton number (n_B) from the hysteresis data (M–H curve) taken at room temperature by using the relation

$$n_B = \frac{\text{molecular weight} \times \text{saturation magnetization}}{5585}. \tag{5}$$

The calculated values of n_B are given in table 1 and are found to decrease with the increase in the concentration of Ti ions, suggesting a decrease in the net magnetic moment of the system.

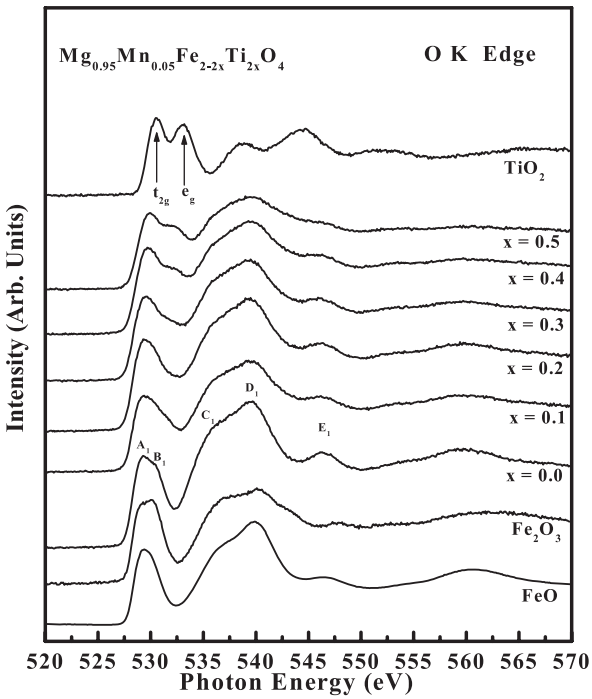

Figure 6. Oxygen (O) K-edge NEXAFS spectra of FeO, Fe_2O_3, TiO_2 and $Mg_{0.95}Mn_{0.05}Fe_{2-2x}Ti_{2x}O_4$ samples.

The magneton number n_B decreases linearly with the Ti substitution, implying that the system follow the Néel's two sublattice model. The observed decrease in n_B can be explained in terms of Néel's two sublattice model of ferrimagnetism given as:

$$n_B^N = M_B(x) - M_A(x), \tag{6}$$

where n_B^N is the Néel magnetic moment per formula unit in μ_B, M_B and M_A are B and A sublattice magnetic moments in μ_B. This can be explained by the fact that Ti^{4+} ions have a strong preference to occupy the octahedral site, thereby reducing the number of magnetic ions at B-sites and thus decreasing the net magnetic moment of the system.

3.4. Near edge x-ray absorption fine structure (NEXAFS)

The O K-edge NEXAFS spectra of $Mg_{0.95}Mn_{0.05}Fe_{2-2x}Ti_{2x}O_4$ ($0 \leqslant x \leqslant 0.5$) along with FeO, Fe_2O_3 and TiO_2 are shown in figure 6. The O K-edge spectra fundamentally reflects a transition from the O 1s core state to the unoccupied O 2p derived states, which are hybridized states with the comparatively narrow 3d and broader 4sp bands of the 3d transition metal ions [29]. The O K-edge spectrum for $x = 0.0$ have low energy features of the so-called pre-edge peaks $A_1(t_{2g})$ and $B_1(e_g)$, constituted by the transitions of O 2p hybridized with Fe 3d states and thus, more sensitive to the changes in the electronic structure caused by charge and orbital ordering effects. These two low energy features are strongly overlapped with each other. The higher energy features above 535 eV are attributed to the oxygen p states hybridized with metal (Fe and Ti) 4s and 4p states. First of all we would like to compare the spectrum of $x = 0.0$ with reference compounds of FeO and Fe_2O_3. The low energy feature of Fe_2O_3 is characterized by a doublet like feature, while FeO is characterized by a singlet like feature. This difference

can be explained by the simple one-electron transition model. For Fe_2O_3, five d electrons are not sufficient to completely occupy the three degenerated t_{2g} orbitals, making both the t_{2g} and e_g orbitals available for the NEXAFS transitions. On the other hand, six d electrons in FeO completely occupy the t_{2g} orbitals, giving rise to only one transition that is related to e_g orbitals. By comparing the spectra of $x = 0.0$ with these reference compounds, it seems that the low energy features look like that of Fe_2O_3 while the high energy features are well matched with that of FeO. In other words, we can say that the spectrum for $x = 0.0$ can be reproduced by the superposition of the spectra of Fe_2O_3 and FeO, which suggests that the 3d orbitals may have more than one symmetry.

It is clear from the O K-edge of NEXAFS spectra that substitution of Ti ions in Mg–Mn ferrite leads to an extensive redistribution of low energy features of Fe 3d (t_{2g} and e_g) states towards the high energy region, which is consistent with results of XRD and electric transport measurements. The high energy features above 535 eV remain unaffected. At 20% substitution of Ti ions, the primitive p–d hybridization is seriously damaged by bringing t_{2g} and e_g orbitals closer to each other. These structural and valent features will definitely influence their magnetic behavior and electronic transport at $x = 0.20$. At higher Ti concentrations $x \geqslant 0.3$, a new spectral feature (∼532 eV) just above the $B_1(e_g)$ starts appearing, which is supposed to be the e_g orbital of the Ti 3d band hybridized with O 2p. Also the high energy features become modified. The feature around 540 eV becomes a broad peak, while another feature at 546 eV has completely vanished. These structural changes may be interpreted in terms of competition between the hybridization of Ti 3d and Fe 3d with O 2p orbitals. Moreover, it is noted that the first peak, which is related to the t_{2g} orbitals starts shifting towards the high energy side with the doping of Ti ions and an overall shift of 0.25 eV is observed. Thus we can say that at higher Ti substitution, the hybridization between O 2p with Ti 3d dominates, which indicates that adding more holes to the system modifies the electronic transport properties of the present compound. The addition of the holes to the system changes the electronic state of Fe, i.e. Fe^{3+} states will be converted to Fe^{2+} states to keep the charge neutrality.

To investigate the valence state of Fe, we have measured the Fe $L_{3,2}$-edge spectra. Figure 7 presents the normalized Fe $L_{3,2}$-edge NEXAFS spectra of $Mg_{0.95}Mn_{0.05}Fe_{2-2x}Ti_{2x}O_4$ ($0 \leqslant x \leqslant 0.5$) along with the reference compounds Fe_2O_3 and FeO. These spectra are primarily due to the Fe 2p–3d hybridization and are strongly influenced by the core–hole potentials. The intensity of these lines can be regarded as a measure of the total unoccupied Fe 3d states. The two broad multiple structures, L_3 and L_2 are well known for reference compounds Fe_2O_3 and FeO. The main difference between the spectra of the reference compounds can be clearly seen at the L_3 feature. The differences are attributed to the variety of 3d electron configurations of Fe ions (Fe^{2+} or Fe^{3+}) and the indication of local symmetry (tetrahedral or octahedral). The L_3 feature of Fe_2O_3 is characterized by a well developed doublet, a small intensity peak marked as A_2 and a main peak marked as B_2, while in FeO the first peak becomes a shoulder of the main peak. These two spectral features in the L_3 region were assigned to Fe t_{2g} and e_g sub-bands, respectively. First of all, we would like to understand the spectrum of the pure compound, i.e. $x = 0.0$. The observed features are similar to the admixture of FeO and Fe_2O_3, which implies that in the pure system Fe is present in both the states (Fe^{2+} and Fe^{3+}). However, the overall NEXAFS profiles are similar between spectra of all compositions and L_3 features closely resemble those of the admixture of FeO and the Fe_2O_3 reference compound, but on substitution of Ti, the shoulder becomes broad. From the nominal composition, the Fe ion should be trivalent Fe^{3+} as well as divalent Fe^{2+}, which is in agreement with some previous works and testified that some Fe^{2+} may also exist during the sintering process. Moreover, the partial reduction of Fe^{3+} ions to Fe^{2+} ions takes place at an elevated firing temperature. In the present studies, the pure system ($x = 0.0$) also has both these states and on substitution of

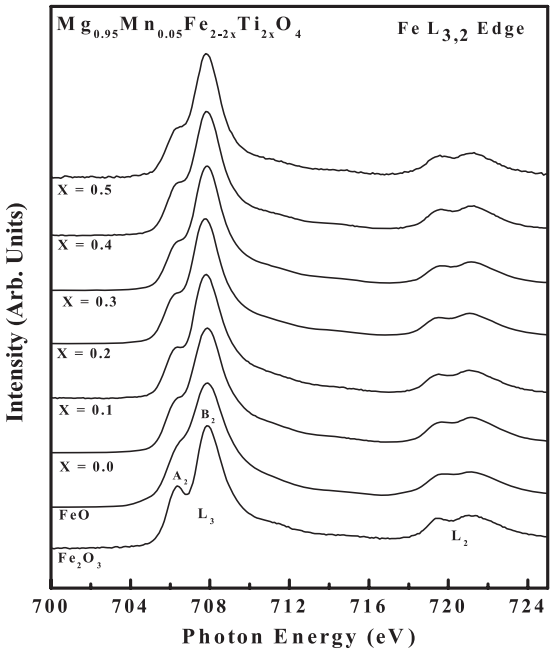

Figure 7. Iron (Fe) $L_{3,2}$-edge NEXAFS spectra of the $Mg_{0.95}Mn_{0.05}Fe_{2-2x}Ti_{2x}O_4$ samples.

Ti^{4+}, Fe^{3+} may be converted to Fe^{2+}. Therefore, in order to clarify the Fe valence state, we have studied Fe K-edge and $L_{3,2}$ edge spectra.

It is a well known fact that the electronic properties of these types of spinel oxide materials are strongly dependent on the cation distribution between the site (A) 'tetrahedral' and the site (B) 'octahedral'. The NEXAFS spectra can be roughly interpreted as the superposition of the independent contribution from Fe^{3+} and Fe^{2+} ions under the octahedral (O_h) and tetrahedral (T_d) local symmetry. Kuiper *et al* [30] reported that the multiplet structures of Fe^{3+} ions are richer than those of Fe^{2+} ions. By looking closely at the observed spectra of the studied compositions, specially the L_3 features, it is not possible to decide for the valence state of the Fe ions based on the present data alone. The L_3 region exhibits a distinctive shoulder together with the main peak and the shape of the shoulder remains more or less the same with the Ti-doping. The only difference we found was that the intensity ratio of main peak to the shoulder peak shows a small decrease as a function of x. There are two possible explanations for this: (a) the ground state is a mixture of $3d^5\underline{L}$ (where $\underline{L}$ denotes a ligand hole) and $3d^6$, or (b) the ground state remains essentially $3d^5\underline{L}$, but the $3d^5$ part contains more than one symmetry. However, we would like to make a few remarks based on the above discussion. If we assume that the ground state of Fe ions is a mixture of Fe^{2+} and Fe^{3+} then there is no electron transfer between Fe^{2+} and Fe^{3+} cations in the entire compositional range, which means that Ti efficiently blocks the electron transfer between $Fe^{2+} \rightarrow Fe^{3+}$ ions, indicating a robust Fe^{3+}/Fe^{2+} channel independent of structural defects. Moreover, because of the soft energy of the x-rays at $L_{3,2}$-edges, electron yield measurements are strongly sensitive to the surface and such measurements are difficult for Fe^{2+} ions, which can be easily oxidized. To avoid surface effects, we used hard x-rays at the K-edge ($1s \rightarrow p$) of Fe ions. The edge energy of x-ray absorption increases typically with increase of the oxidation number of the species under study. Figure 8 shows the Fe K-edge NEXAFS spectra of

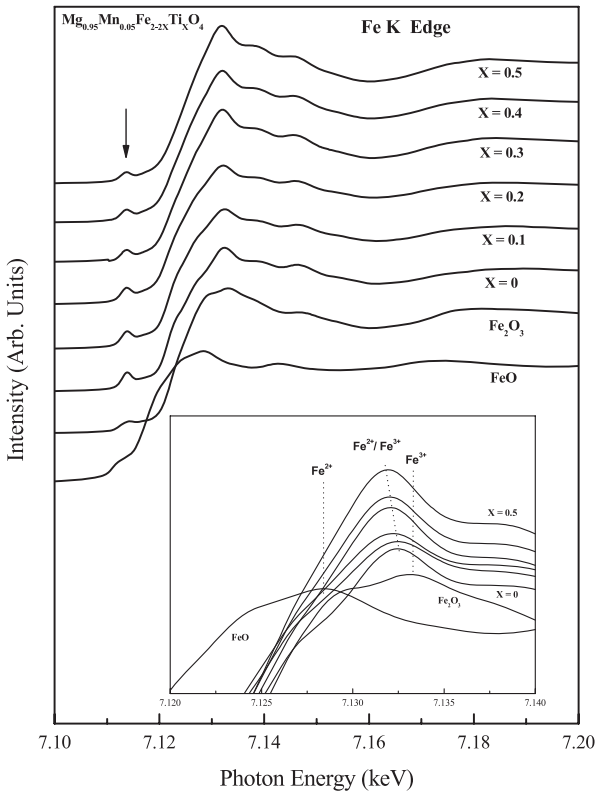

Figure 8. Iron (Fe) K-edge NEXAFS spectra of the $Mg_{0.95}Mn_{0.05}Fe_{2-2x}Ti_{2x}O_4$ samples, where the inset provides an extended view of the main crest position.

$Mg_{0.95}Mn_{0.05}Fe_{2-2x}Ti_{2x}O_4$ ($0 \leqslant x \leqslant 0.5$) along with FeO and Fe_2O_3 for comparison. The pre-edge peak near 7111 eV (marked by an arrow) results from the 1s to 3d transition and has a significant intensity because of 3d–2p orbital mixing [31]. In general, the pre-edge centroid position depends strongly on the Fe oxidation state, whereas the pre-edge intensity is mostly influenced by the Fe coordination geometry. Low intensities refer to the geometries with center of symmetry (e.g. octahedral); high intensities refer to non-centrosymmetric geometries (e.g. tetrahedral) [32]. The pre-edge peak of the studied system having high intensity as compared to standard compounds, suggests an increased number of 3d vacancies on which one may excite the core electron. At the same time, the pre-edge intensity decreases with Ti-doping due to the distortion of the Fe site from tetrahedral towards octahedral symmetry. The inset in figure 8 represents the extended view of the main edge region of the Fe K-edge spectra. The main edge position at ∼7133 eV which is very close to the standard Fe_2O_3 edge confirms that Fe^{3+} is the dominant oxidation state, with the Fe^{2+} component being too low to be detected by L-edge NEXAFS (as discussed above). As evident, all the samples show the Fe^{2+}–Fe^{3+} mixed-valent states and the main crest position moves towards lower energies with the substitution of Ti ions. Thus, we can say that Fe ions are in the mixed-valent states (Fe^{2+}–Fe^{3+}) and the substitution of Ti^{4+} ions causes more Fe^{2+} components in the system. These spectral differences reflect the variation in the structural environment of Fe^{2+} and Fe^{3+}, respectively.

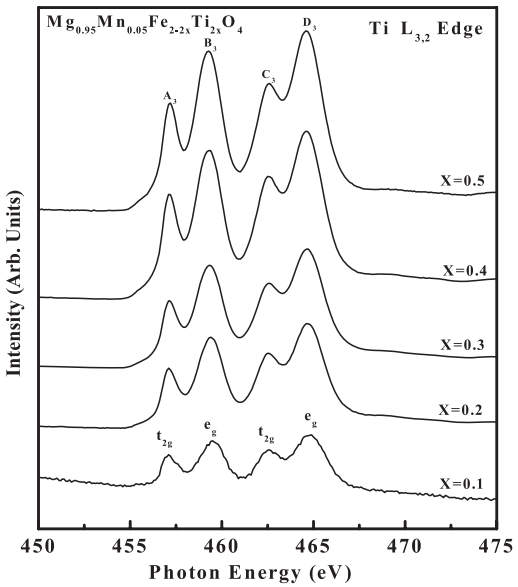

Figure 9. Titanium (Ti) $L_{3,2}$-edge NEXAFS spectra of the $Mg_{0.95}Mn_{0.05}Fe_{2-2x}Ti_{2x}O_4$ samples.

Figure 9 shows the Ti $L_{3,2}$-edge NEXAFS spectra of the entire compositions. The spectra are split into L_3 and L_2 regions by the spin–orbit interactions, reflecting transitions of Ti 2p core electrons into Ti 3d states in the conduction bands. The L_2-edge features are broadened compared to those of the L_3 edge, owing to the increased Coster–Kroning Auger decay channel [33] for the L_2 edge. The four intense peaks distributed from 456 to 466 eV can be assigned as $2p_{3/2}t_{2g}$ (A_3), $2p_{3/2}e_g$ (B_3), $2p_{1/2}t_{2g}$ (C_3), and $2p_{1/2}e_g$ (D_3) based on the calculation of the dipole transition probability from Ti $3d^0$ to $2p^53d^1$. Indeed, atomic multiplet calculations of de Groot *et al* [34] have suggested that these multiple peaks are mainly due to strong Coulomb interactions between poorly screened Ti 3d electrons and the Ti 2p core hole. It is known that the separation between the two main peaks in the L_3 (peak A_3 and B_3) and L_2 (peak C_3 and D_3) edge is associated with the crystal-field splitting modified by strong exchange interaction. de Groot *et al* [34] have reported a series of Ti^{4+} 2p-edge absorption spectra calculated for different crystal-field strengths. As can be seen, there is no main difference in the absorption spectra of all the compositions, except the gain in spectral weight of each of the peaks, indicating an increase in the Ti concentration. We compared the measured spectra of all compositions with the $L_{3,2}$ titanium absorption spectra of the $SrTiO_3$ compound, which possessed practically perfect octahedral site symmetry for titanium atoms. Also, the separations between various observed peaks are well matched with the Ti^{4+} 2p-edge spectra in octahedral symmetry calculated by de Groot *et al* for this and other mixed perovskite compounds. It is estimated that the 10 Dq for this entire series is around 2.1 eV. Therefore, this result implies that the valency of Ti remains unchanged at 4+.

All the above NEXAFS results suggest that substitution of Ti ions in Mg–Mn ferrite modifies the electronic structure of these materials to a large extent. The conversion of Fe^{3+} to Fe^{2+} states as indicated by magnetization, and electric transport studies is confirmed by Fe K-edge NEXAFS spectra. The increase in unit cell volume calculated from XRD data also confirms the same.

4. Summary

In summary, we have successfully synthesized polycrystalline bulk samples of $Mg_{0.95}Mn_{0.05}Fe_{2-2x}Ti_{2x}O_4$ ($0 \leqslant x \leqslant 0.5$) by a standard solid-state reaction technique. The XRD analysis of $Mg_{0.5}Mn_{0.05}Fe_{2-2x}Ti_{2x}O_4$ indicates that all samples exhibit a single phase nature with structural transition from cubic spinel to tetragonal due to the Ti substitution. An increase in the unit cell volume also confirms that, with the substitution of Ti ions, the conversion from Fe^{3+} to Fe^{2+} takes place to maintain the charge neutrality in the system. The dispersion behavior of the dielectric constant as a function of frequency has been explained according to interfacial polarization as predicted by the Maxwell–Wagner and Koop's phenomenological theory. The composition dependent dielectric constant is found to increase with increasing Ti ion concentration up to 20% ($x = 0.2$) and has been explained in terms of hopping (exchange) of electrons between Fe^{2+} and Fe^{3+}, which indicates that the polarization in these materials is similar to the conduction process in ferrites. It is observed that AC and DC conductivity also increase with substitution up to $x = 0.2$, after that it decreases systematically. The exponent 's' of the power law behavior of AC conductivity ($\sigma_{AC} = A\omega^s$), which refers to the measure of charge correlation, was calculated and found to be in the range 0.5–0.8, implying a strong correlation of electrons in these systems. The DC magnetization study infers that all the samples exhibit a ferrimagnetic behavior at or above room temperature and saturation of magnetization decreases with increasing concentration of Ti ions. A decrease in the saturation of magnetization with the substitution of Ti is explained in terms of Néel's two sublattice model of ferrimagnetism. The NEXAFS study clearly indicates that the doping of Ti ions modifies the electronic structure of these systems. The O K-edge spectra of undoped ($x = 0.0$) indicates that the low energy feature resembles that of Fe_2O_3. However, after the Ti-doping, it is clearly seen that the doublet feature of Fe_2O_3 changes to one like FeO. This means that Fe^{3+} is changing to Fe^{2+}, which is consistent with the transport study. The Fe K- and $L_{3,2}$-edge spectra also confirmed that the substitution of Ti^{4+} ions leads to the conversion of Fe^{3+} to Fe^{2+}. The Ti $L_{3,2}$-edge NEXAFS spectra of the entire range of compositions split into L_3 and L_2 regions by the spin–orbit interactions, reflecting transitions of Ti 2p core electrons into Ti 3d states in the conduction bands. The separation between various observed peaks is well matched with Ti^{4+} 2p-edge spectra in O_h symmetry. The estimated value of 10 Dq for this entire series is approximately 2.1 eV which implies that the valency of Ti in all compositions remains as 4+ states. Finally, we can say that the substitution of Ti modified the structural, magnetic, electrical, and electronic properties and also gave these materials multiferroic properties, which are in good agreement with our earlier reported results [35, 36].

Acknowledgments

One of the authors (Shalendra Kumar) would like to thank CSIR for financial support in the form of Senior Research Fellowship (SRF). The author is also thankful to the Inter-University Accelerator Centre, New Delhi for providing the experimental facilities.

References

[1] Brabers V A M 1995 *Handbook of Magnetic Materials* vol 8, ed K H J Buschow (Amsterdam: Elsevier)
[2] Bhargava S C and Zeman N 1980 *Phys. Rev.* B **21** 1717
[3] Muralidharan K, Srivastava J K, Moratha V R and Vijayaraghavan R 1985 *J. Phys. C: Solid State Phys.* **18** 5897
[4] Brand R A, Lauer J and Herlach D M 1984 *J. Phys. F: Met. Phys.* **14** 555–64
[5] Dormann J L and Nogues M 1990 *J. Phys.: Condens. Matter* **2** 1223

[6] Dormann J L, Harfaouni M E I, Nogues M and Love J 1987 *J. Phys. C: Solid State Phys.* **20** L161
[7] Daniels J M and Rosencwaig A 1970 *Can. J. Phys.* **48** 2857
Daniels J M and Rosencwaig A 1970 *Can. J. Phys.* **48** 2868
[8] Rosencwaig A 1970 *Can. J. Phys.* **48** 381
[9] Dormann J L 1980 *J. Phys. C: Solid State Phys.* **41** 175
[10] Nogues M, Dormann J L, Pernn M, Siment W and Gibrat P 1980 *IEEE Trans. Magn.* **15** 1729
[11] Dormann J L and Renaudin P 1980 *Ferrites, Proc. Int. Conf. (Japan, Sept. 1980)* p 156
[12] Chae K P, Kim W K, Lee S H and Lee Y B 2001 *J. Magn. Magn. Mater.* **232** 133–8
[13] Suryavanshi S S, Jadav C N, Patil S A and Sawant S R 1989 *Mater. Res. Bull.* **24** 1201
[14] Brand R A, Georges-Gibert H, Hubsch J and Heller J A 1985 *J. Phys. F: Met. Phys.* **15** 1987–2007
[15] Suryavanshi S S, Patil R S, Patil S A and Sawant S R 1991 *J. Less-Common Met.* **168** 169
[16] Reddy M B and Reddy V 1990 *Phys. Status Solidi* a **120** 575
[17] Prakash C and Bijal J 1985 *J. Less-Common Met.* **107** 51
[18] Krishnan R V and Banarjee A 1999 *Rev. Sci. Instrum.* **70** 85
[19] Heikes R R and Johnson W D 1957 *J. Chem. Phys.* **26** 582
[20] Maxwell J 1873 *Electricity and Magnetics* vol 1 (London: Oxford University Press) section 328
[21] Koops C 1951 *Phys. Rev.* **83** 121
[22] Reddy P and Rao T 1982 *J. Less Common Met.* **86** 255
[23] Smit J and Wijn H 1959 *Ferrites* (New York: Wiley) p 369
[24] Isamail H, El Nimr M, Abo El Ata A, El Hiti M, Ahmed M and Murakhowskii A 1995 *J. Magn. Magn. Mater.* **150** 403
[25] Elliott S R 1987 *Adv. Phys.* **36** 135
[26] Ghosh A 1992 *Phys. Rev.* B **45** 11318
[27] Mazen S A 1972 *Mater. Chem. Phys.* **62** 1522
[28] Mazen S A and Dawoud H A 2003 *Mater. Chem. Phys.* **82** 557
[29] Asokan K *et al* 2001 *J. Phys.: Condens. Matter* **13** 3311
[30] Kuiper P, Kruizinga G, Ghijsen J, Sawatzky S A and Verweij H 1989 *Phys. Rev. Lett.* **62** 221
[31] Arrio M A, Rossano S, Brouder Ch, Galoisy L and Calas G 2000 *Europhys. Lett.* **51** 454
[32] Wilke M, Partzsch G M, Bernharett R and Lattard D 2005 *Chem. Geol.* **220** 143
[33] Thole B T, van der Laan G, Fuggle J C, Sawatzky G A, Karnatak R C and Esteva J M 1985 *Phys. Rev.* B **32** 5107
[34] de Groot F M F, Fuggle J C, Thole B T and Sawatzky G A 1990 *Phys. Rev.* B **41** 928
[35] Kumar S, Alimuddin, Kumar R, Dogra A, Reddy V R and Banerjee A 2006 *J. Appl. Phys.* **99** 08M910
[36] Kumar S, Kumar R, Sharma S K, Reddy V R, Banerjee A and Alimuddin 2007 *Solid State Commun.* **142** 706–9